OnLine Journal of Earth Sciences 5 (2): 12-21, 2011
ISSN: 1991-7708
© Medwell Journals, 2011

Impact of the Astronomical Potential Forcing on the Local Solution

Imen Ben Jaber, Jihene Abdennadher and Moncef Boukthir
UR1304, Institut Preparatoire aux Etudes d'Ingenieur de Tunis, University of Tunis,
2 Rue Jawaher Lel Nehru, 1089 Montfleury, Tunisia

Abstract: We have used a high-resolution barotropic tidal model to predict tidal elevations and currents in the Tunisian shelf and the Strait of Sicily (Mediterranean sea). Model performance was evaluated with respect to tide gauge measurements. General features for the various semidiurnal constituents are nearly similar to each other with maximum amplitude in the Gulf of Gabes. The modelled tidal characteristics are in good agreement with observations and previous global solutions. Nevertheless, it seems that the only forcing by elevation at the open boundaries is not able to reproduce the intensity of the observed resonance in the Gulf of Gabes, since the amplitude is underestimated. When the potential forcing is added, the solution is much better in term of amplitude. Indeed, the maximum modelled amplitude (51.7 cm) is very close to the observed one (51.1 cm). The potential forcing enhances the amplitude and places correctly the amphidromes. It seems that the impact of the potential forcing is particularly important within the semidiurnal frequency which is the resonance frequency in the Gulf of Gabes.

Key words: Tide, potential forcing, energetics, Mediterranean sea, amplitude, Tunisia

INTRODUCTION

Although, the tidal ranges in the Mediterranean sea are small, they may significantly contribute to the changes in sea level in some locations. For example in the Gulf of Gabes, tides are responsible for most of the observed sea level variability and may reach 1.5 m. Moreover, it is suggested that some of the energy from the tide might be feeding part of the energetic low-frequency circulation observed in the Mediterranean through mixing and tidal rectification mechanisms (Candela *et al*., 1995). While the tidal future of the whole Mediterranean sea have been well documented (Defant, 1961; Sanchez *et al*., 1992; Lozano and Candela, 1995; Tsimplis *et al*., 1995), the local solutions have not. To the knowledge, only a few numerical studies are devoted to investigate the local solutions in the Mediterranean. The 1st realistic study was conducted by Molines (1991) in the frame of Topex/Poseidon altimeter calibration and used a finite difference 2D barotropic model to simulate the tides in the Strait of Sicily.

The 2nd was conducted by Tsimplis (1994) for the purpose of investigating the tidal oscillations in the Aegean and Ionian seas. Recently, Abdennadher and Boukthir (2006) have investigated the energetic of the barotropic tides in the Sicily strait and the adjacent areas. In the South of the Mediterranean, measurements of tidal elevations and particularly currents are very rare. The few available tide gauge data are scattered over the continental shelves but there is no information in the central area, except in a few islands. In this context, numerical models provide the most effective method for improving the knowledge of tides in this region. We have therefore, used a 2D version of a three-dimensional sigma coordinate model, the Regional Ocean Modeling System (ROMS) to investigate the barotropic tidal components in the Gulf of Gabes and adjacent area. It is important to note that the highest tidal amplitude in the Mediterranean sea is observed in the Gulf of Gabes as a result of resonance phenomena.

Furthermore, it was suggested that about 70% of tidal energy dissipation in the Mediterranean occurs in the Gulf of Gabes which accounts for only 5% of whole area of the Mediterranean (Tsimplis *et al*., 1995). It is well known that for the local solution purpose, the motion is forced in the model by tidal variations in the open boundaries. The purpose of this study is primary to check whether the potential forcing is important in successfully reproducing the resonance observed in the Gulf of Gabes.

To this end, we have implemented the body earth tide and associated perturbations of the astronomic tide-generating potential as well as the load tide in the model in which the resolution of (1/24°×1/24°) is higher than all of the previous models. We believe that this high

Corresponding Author: Imen Ben Jaber, UR1304, Institut Preparatoire aux Etudes d'Ingenieur de Tunis, University of Tunis, 2 Rue Jawaher Lel Nehru, 1089 Montfleury, Tunisia

resolution contributes to improve the results. We also think that it is important to evaluate the differences between local solution and global one as predicted by global models used to filter the tidal signal from the altimetric data. Indeed, yet today the existing global numerical models do not succeed in describing the tidal characteristics with a sufficient accuracy in all areas, particularly over the continental shelves.

Finally, this kind of study is important not only for navigational and coastal purposes but also for understanding the marine pollution problem observed in the Gulf of Gabes. Since, a good knowledge of the tidal currents is helpful for successfully simulating spatial and temporal distribution of the pollutant which would be precious information for many environmental studies. Indeed, it is established that tides play significant roles in ocean mixing (Munk and Wunsch, 1998).

Equations of barotropic tide: According to the fundamental law of the dynamics, the temporal variation of the impulse by unity of volume of a fluid particle associated with a viscous fluid in uniform rotation around the axis of the earth is equal to the sum of the volume strengths and the strengths of frictions being applied on the fluid:

$$\rho\left(\frac{D\vec{u}}{Dt}+2\vec{\Omega}\wedge\vec{u}\right)=-\vec{\nabla}P+\vec{f}_{vol}+\vec{F}_f \quad (1)$$

The local equation of continuity for a fluid is given by:

$$\frac{\partial\rho}{\partial t}+\vec{\nabla}.(\rho\vec{u})=0 \quad (2)$$

Where:

ρ = The density of fluid
$\vec{u}=(u,v,w)$ = The speed of a fluid particle
$\vec{\Omega}$ = the angular acceleration relative to the rotation of the earth around its axis
$\vec{\nabla}$ = the gradient operator
$-\vec{\nabla}P$ = The resultant volume of the strengths of pressure being applied on a fluid particle
$\vec{f}_{vol}$ = The volume strengths which include the strengths due to the fields of attraction gravitational and all other volume strengths which can exist in the fluid
$\vec{F}_f$ = The volume strengths not conservatives representing the effects of friction such as the strengths of viscosity

The instantaneous water depth is given by:

$$h = H(x, y) + \zeta(x, y, t)$$

Where:

H (x, y) = The ocean depth at rest
ζ (x, y, t) = The free surface elevation

By integrating the equation of motion (Eq. 1) and the equation of continuity (Eq. 2) on the depth and by using the boundary conditions at the bottom and on surface, we obtain:

$$\frac{\partial\vec{u}}{\partial t}+(\vec{u}.\vec{\nabla})\vec{u}+2\vec{\Omega}\wedge\vec{u}=-g\vec{\nabla}\zeta-\frac{\vec{\tau}_b}{h}+\vec{D}_m \quad (3)$$

$$\frac{\partial h}{\partial t}+\vec{\nabla}.(h\vec{u}) = 0 \quad (4)$$

Where:

$\vec{u}$ = Indicates the barotropic velocity
$\vec{\tau}_b$ = The bottom stress
$\vec{D}_{hu}$ = The horizontal diffusion term integrated over the depth

Knowing that:

$$h = H + \zeta$$

Where, H is constant, the Eq. 4 becomes:

$$\frac{\partial\zeta}{\partial t}+\vec{\nabla}.(h\vec{u}) = 0 \quad (5)$$

If the tide-generating potential is introduced in the equation of motion, Eq. 3 becomes:

$$\frac{\partial\vec{u}}{\partial t}+(\vec{u}.\vec{\nabla})\vec{u}+2\vec{\Omega}\wedge\vec{u}=-g\vec{\nabla}\left(\zeta-\zeta_{pot}\right)-\frac{\vec{\tau}_b}{h}+\vec{D}_{hu} \quad (6)$$

Where, ζ_{pot} indicates the variations of the height of water engendered by the generative potential of tide.

Model setup

Model description: In this study, we use the barotropic version of the Regional Oceanic Modelling System (ROMS). ROMS solves the primitive equations in an earth-centred rotating environment based on the Boussinesq approximation and hydrostatic vertical momentum balance. It uses stretched, terrain-following coordinates in the vertical and orthogonal curvilinear coordinates in the horizontal. ROMS is a split-explicit, free-surface oceanic model where short time steps are used to advance the surface elevation and barotropic momentum equations with a much larger time step used for temperature, salinity and baroclinic momentum. ROMS employs a special 2-way time-averaging procedure for the barotropic mode which satisfies the 3D continuity

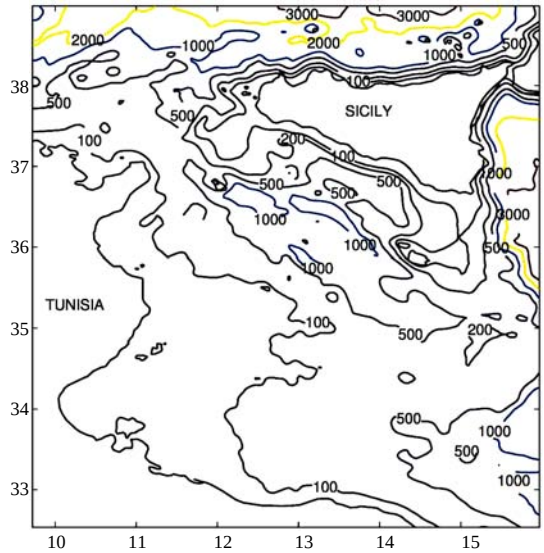

Fig. 1: Bathymetry in the Tunisian area and the Strait of Sicily

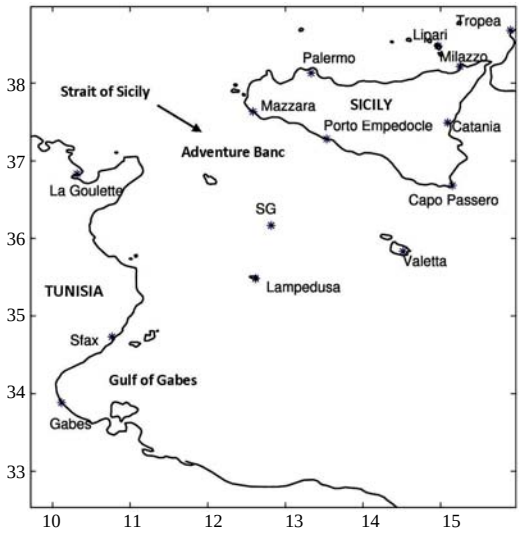

Fig. 2: The locations (stars) of the tide gauges data used for the validation of the model results

equation. For further details and more complete description of the model, the reader is referred to Shchepetkin and McWilliams (2003).

Model grid and bathymetry: The region covered by the present study includes the Tunisian shelf and the Sicily strait. The model domain (Fig. 1) extends from 9.7°-16°E and from 32.5°-39°N. The horizontal model resolution is 1/24° in both longitudinal and latitudinal directions which corresponds to 3.6 km in the longitude and 3.6-3.9 km in the latitude. A grid spacing in σ is used in the vertical with 20 vertical levels. For numerical stability, the time-step of integration Δt was chosen as 7.5 sec in order to satisfy the CFL condition $\Delta t < \Delta s/\sqrt{2gh}$ where, Δs is the minimum grid length.

The model bathymetry is deduced from Smith and Sandwell (1997) topography database by a bilinear interpolation of the depth data onto the model grid. The water depths <10 m are set to 10 m in the model. The resulting bathymetry is showed in Fig. 1. It shows the main features of the modelled are geometry which is mainly characterised by the Tunisian shelf and the Adventure Bank where depths are <100 m and a much deeper Eastern area with a maximum depth of about 3000 m.

Simulation strategy: Tidal forcing was implemented by setting the elevations of the major constituents in the region (M_2, S_2, N_2, K_1 and O_1) along the four open boundaries with the coefficients taken from a two-dimensional gravity-waves model (Hereinafter referred to as Mog2d) of the Mediterranean (F. Lyard, personal communication). For each constituent i, the associated elevation ζ_i is defined by:

$$\zeta_i(t) = f_i A_i \cos[\omega_i(t-t_0) + u_i + v_i - G_i] \quad (7)$$

Where:

A_i and G_i = The amplitude and the phase lag relative to Greenwich of the equilibrium constituent i

f_i and u_i = Nodal factors for amplitude and phase

v_i = The phase of the equilibrium constituent i at Greenwich time $t = t_0$ being January 1, 1950 (Table 1)

Table 1: Angular speed and nodal factors for the calculation of the equilibrium tide. The origin of time ($t = t_0$) corresponds to January 1, 1995

Composantes	Speed (°/h)	f	u (°)	v (°)
M_2	28.98410400	0.964	359.547	71.395
S_2	30.00000000	1.000	0.000	0.000
N_2	28.43972950	0.964	359.547	200.162
K_1	15.04106860	1.111	358.385	10.081
O_1	13.94303557	1.180	1.807	61.314

The bottom frictional stress is represented by a drag formulation with a quadratic drag coefficient C_D. Sensitivity tests in which C_D varied from 10^{-3} to 3×10^{-3} allowed us to adjust C_D to 2×10^{-3}. This value which corresponds to the best fit for amplitudes and phases measured at different coastal stations (Fig. 2) is within the range of observed values (10^{-3} to 3×10^{-3}) reported by Gallagher and Munk (1971) and it is similar to those used in other numerical models (e.g., Parker, 1991; Le Provost *et al*., 1994).

In order to assess the impact of the potential forcing on the quality of the simulations, researchers carried out two series of experiments. Motion was forced in the model by tidal elevations along the open boundaries (experiment E1, hereinafter) and by both tidal variations in the open boundaries and tide-generating forces acting over the interior (experiment E2, hereinafter). For E1, the model integrates the Eq. 3 and 5 and for E2, it integrates the Eq. 5 and 6.

For both two experiments, the model was integrated forward in time from initial conditions of zero elevation and motion for 60 days with data saved at 20 mn intervals. The 1st 30 days which were influenced by the initial conditions were discarded and the subsequent final 30 days were harmonically analysed to obtain the amplitude and phase for elevations and currents. It is important to note that the considered constituents can be accurately separated from each other by the harmonic analysis of a time series >1 month.

Data validation: The basic data used in the validation of the model results comes mainly from the tide gauge measurements. The tide-gauge data were collected from several sources, namely Molines (1991) and Tsimplis *et al.* (1995). Although, tide gauge data are subject to measurement errors, they provide useful independent information about the performance of the tidal model solution. Nevertheless, what should be remembered is that any discrepancies between the model results and the observed tides (which are only estimates of the tides) could be due to either model inaccuracies or errors in the estimation of the observed tides. In addition, the data location does not coincide with a model grid point introducing further uncertainties.

The model amplitude and phase are compared to tide gauge data which consist of time series elevation at 14 coastal stations distributed over the domain (Fig. 2). We have selected these stations for their regular separation in order to cover the domain. We have omitted some other stations because the lengths of their time series are not sufficiently long to allow a proper separation of the different tidal constituents. Among all the selected stations, there is only one offshore tide gauge station named SG (Astraldi *et al.*, 1987).

RESULTS

The computed amplitude and phase for M_2 component are shown in Fig. 3 for both experiments E1 and E2. The general features of amplitude and phase for both experiments are similar. The amplitude reaches its maximum in the Gulf of Gabes and it decreased moving towards the north of the Strait of Sicily and towards the deep eastern region. This means that the model reproduce qualitatively the amplification of the amplitude in the Gulf of Gabes. Nevertheless, the maximum amplitude of M_2 component for E1 experiment does not exceed the half of the observed value.

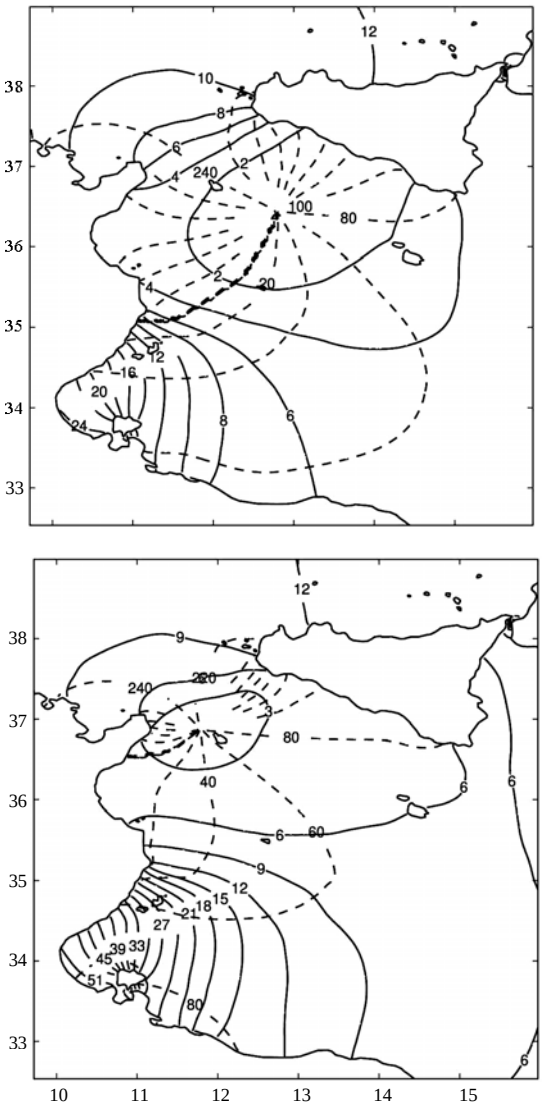

Fig. 3: Amplitude contours every 2 cm (solid line) and phase contours (dashed line) every 20° of the M_2 constituent for E1 (left) and E2 (right) experiments

When the potential forcing and the load tide are introduced (experiment E2), the amplitude in the gulf of Gabes is about 51.7 cm (Table 2) which suggests that the strong resonance observed in this Gulf is well reproduced in the simulations since, the observed value

Table 2: Observed Amplitude (A_{ob}) and Phase (P_{ob}) and modeled Amplitude (A_{Ei}) and Phase (P_{Ei}) for M_2 elevation at 14 coastal locations

Stations	A_{ob}	A_{E1}	A_{E2}	P_{ob}	P_{E1}	P_{E2}
La goulette	8.0	9.9	8.3	249.4	244.6	248.4
Sfax	41.6	16.0	36.1	76.1	29.1	62.3
Gabes	51.1	24.0	51.7	79.1	48.6	78.7
SG	4.8	0.5	4.4	50.0	23.1	62.1
Palermo	11.3	11.8	12.4	236.3	227.3	227.2
Mazzara	4.3	5.6	6.2	127.8	193.7	165.3
Po. Emp	4.9	1.5	4.6	73.0	131.6	92.5
Valetta	6.0	2.8	5.7	64.0	63.9	68.1
C. passero	6.7	4.7	6.2	61.6	69.3	71.3
Lampedusa	7.6	2.0	6.4	42.5	18.5	51.7
Catania	6.5	4.6	6.1	56.4	66.8	73.0
Tropea	14.6	12.3	13.7	242.2	226.8	228.6
Milazzo	12.0	12.2	13.4	234.0	227.4	229.2
Lipari	12.0	12.2	13.3	232.0	227.5	228.8

Table 3: Observed Amplitude (A_{ob}) and Phase (P_{ob}) and modeled Amplitude (A_{Ei}) and Phase (P_{Ei}) for M_2 elevation at 14 coastal locations

Stations	A_{ob}	A_{E1}	A_{E2}	P_{ob}	P_{E1}	P_{E2}
La goulette	3.0	3.6	3.0	274.4	271.1	279.9
Sfax	26.7	15.6	27.0	103.1	66.7	88.8
Gabes	36.4	23.8	39.3	107.3	85.8	106.2
SG	3.1	1.8	3.7	57.0	61.6	71.2
Palermo	4.3	4.5	4.8	259.6	246.7	245.8
Mazzara	1.8	1.7	2.5	102.8	184.0	151.7
Po. Emp	3.5	1.7	3.5	71.4	84.6	87.6
Valetta	3.7	2.3	3.7	71.0	74.5	78.0
C. passero	3.5	2.4	3.1	67.3	78.4	78.2
Lampedusa	4.9	2.6	4.8	56.6	58.0	68.3
Catania	3.5	2.4	3.0	61.9	77.8	80.9
Tropea	5.3	4.8	5.5	264.2	246.4	246.4
Milazzo	4.7	4.7	5.3	252.0	247.0	247.3
Lipari	4.5	4.7	5.3	254.0	247.0	247.0

is about 51.1 cm. For both experiments, there is one amphidrome for M_2 component located near the vicinity of the Pantelleria island with the phase rotating anticlockwise around the amphidrome (Fig. 3). Another difference between the two experiments consists of the position of the amphidromic point of M_2. Indeed in E1 experiment, the amphidromic point is located at the South-East of the Pantelleria island whereas it is located slightly in the North-West of this island for E2 experiment. Mosetti *et al.* (1983) placed it at the North of this island and Molines (1991) also found a difference in the location of the amphidrome, having it at 20 km North-West of Pantelleria island. Whatever, these uncertainties are, they do not mask the fact that the amphidrome for M_2 component may be seen in the vicinity of the Pantelleria island. It seems that the position of the amphidrome is more realistic for E2 than E1 experiment. The general features of the other simulated semidiurnal components (S_2 and N_2) are similar to those of the M_2 but with reduced amplitudes, particularly for N_2.

The maximum amplitude for S_2 is also located in the Gulf of Gabes with a gradual reduction toward the East (Fig. 4). Again, the amplitudes of S_2 and N_2 estimated by E2 experiment are more close to the observation than those estimated by E1 experiment (Table 3 and 4), particularly in the resonance region (the Gulf of Gabes). Indeed in the Sfax station, the observed amplitude of elevation is 26.7 cm and it is about 27.0 cm for E2 and only 23.3 cm for E1. The same conclusion holds for the 2nd station in the resonance region (Port of Gabes). The amplitude for N_2 in the Gulf of Gabes is much weaker than that of the other semidiurnal constituents; only about 6.5 cm for E2 experiment (Fig. 5). Elsewhere, the amplitude is very weak and it does not >3 cm. It should be noted that the amplitude of semidiurnal components declines rapidly from the port of Gabes to the end of the Gulf of Gabes for all the semidiurnal constituents. The amphidromic point of the S_2 component as simulated by

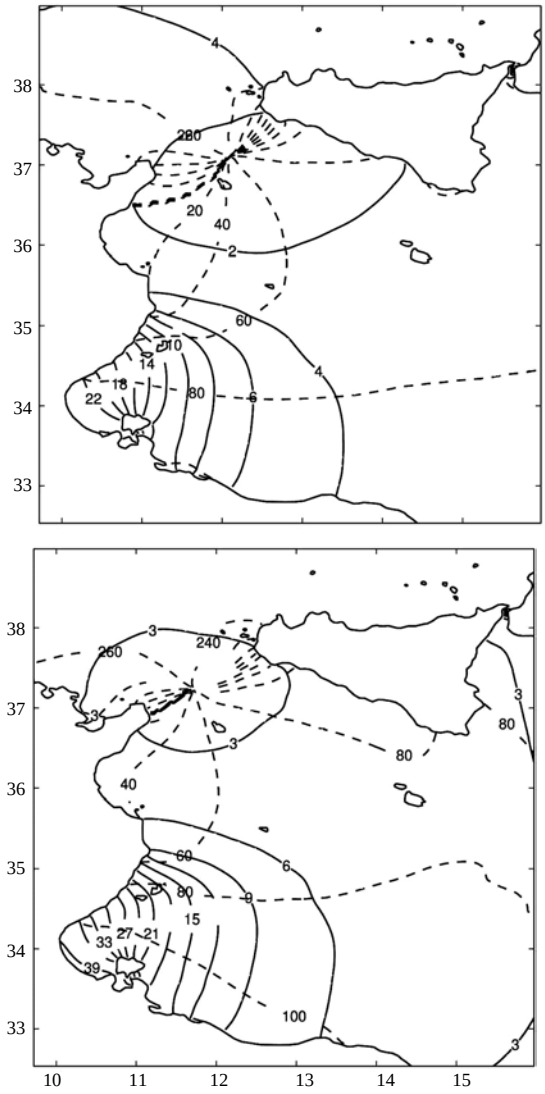

Fig. 4: Amplitude contours every 2 cm (solid line) and phase contours (dashed line) every 20° of the S_2 constituent for E1 (left) and E2 (right) experiments

Table 4: Observed Amplitude (A_{ob}) and Phase (P_{ob}) and modeled Amplitude (A_{Ei}) and Phase (P_{Ei}) for N_2 elevation at 14 coastal locations

Stations	A_{ob}	A_{E1}	A_{E2}	P_{ob}	P_{E1}	P_{E2}
La goulette	2.0	2.00	1.7	221.4	234.4	235.3
Sfax	6.2	1.70	4.3	69.3	18.2	60.2
Gabes	8.8	2.50	6.5	78.8	38.8	79.0
SG	-	0.20	0.5	220.3	198.6	86.2
Palermo	2.3	2.40	2.5	222.7	220.3	220.7
Mazzara	1.1	1.30	1.4	128.9	190.5	171.0
Po. Emp	0.8	0.40	0.8	88.7	162.5	116.6
Valetta	0.9	0.40	0.8	85.0	79.9	76.6
C. passero	1.3	0.80	1.1	60.0	71.9	74.1
Lampedusa	1.0	0.06	0.7	51.3	323.8	60.4
Catania	1.1	0.80	1.1	62.1	76.7	74.7
Tropea	-	2.50	2.7	68.6	220.0	222.6
Milazzo	2.1	2.50	2.7	221.6	220.6	223.0
Lipari	2.4	2.50	2.7	218.6	220.6	222.5

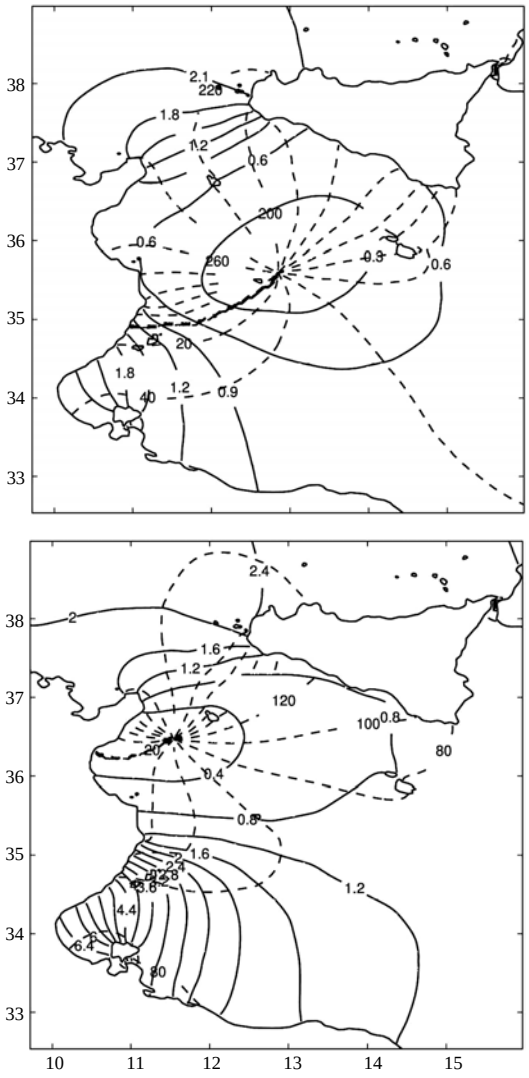

Fig. 5: Amplitude contours every 0.3 cm (solid line) and phase contours (dashed line) every 20° of the N_2 constituent for E1 (left) and E2 (right) experiments

E2 is situated in the Cape Bon (Tunisia)-Mazzara (Sicily) line with the phase rotating anticlockwise. It is slightly shifted to the North (0.3°) in comparison with that of M_2. E1 places the amphidrome slightly 0.5° at the East of that of E2 experiment. For N_2, there is also one amphidrome located in the vicinity of Pantelleria island, slightly in the South of the M_2 amphidrome for E2 experiment. Nevertheless, E1 experiment places the N_2 amphidromic point in the South-East of that of E2 experiment. The scarcity of measurements and the differences between the previous studies make difficult any attempt to check the accuracy of the solution in terms of positioning the amphidromic points.

Nevertheless, the positions of amphidromic points for all simulated components simulated by E2 experiment are more close to those reported in the literature (Molines, 1991; Abdennadher and Boukthir, 2006) than E1 experiment. The amplitude and phase distributions of the major diurnal K_1 component for both experiments E1 and E2 shown in Fig. 6 are nearly similar. The maximum and minimum are nearly situated at the same places for E1 and E2 experiments. The largest elevations are due to the semidiurnal components since, the maximum diurnal amplitude does not >5 cm. The Adventure Bank is the only area where large amplitudes up to 4 cm, exist. This maximum is observed in the North-West of Sicily which is far from the Gulf of Gabes, confirming thus that the resonance in the basin is within the periods of the semidiurnal components.

This local maximum produces strong diurnal currents in the area, probably the signature of coastal trapped waves in this area as suggested by the phase pattern around the Western extremity of Sicily. In the East basin, the amplitudes are characterised by a zonal distribution. The maximum elevation amplitude is located at the same places for both experiments.

Another important feature for K_1 is the presence of one amphidromic point located in the vicinity of Linosa island with the phase (Fig. 6) rotating anticlockwise around the amphidrome. Nevertheless, the experiment E1 places the amphidromic point of K_1 at 0.5° East of that of E2 experiment. Globally, the potential forcing seems to have a minor impact on the simulation of diurnal component (Table 5) which is not the frequency of the resonance in the modelled area. In contrast, the results suggest that the potential forcing and the load tide have a significant impact in the resonance area within the semidiurnal components.

Validation of the simulated tide against tide gauge data: To asses more the impact of the potential forcing and the load tide in reproducing with realism the principal

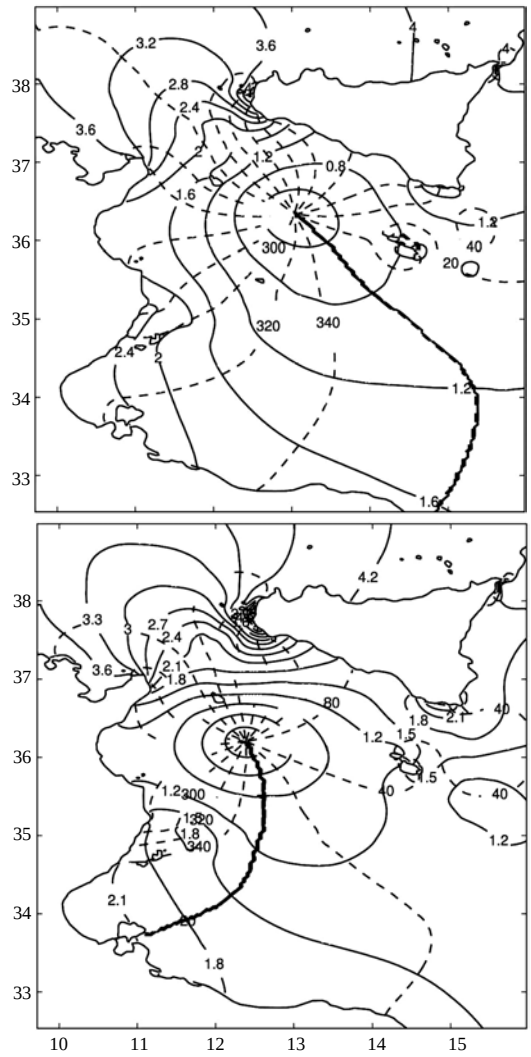

Fig. 6: Amplitude contours every 0.4 cm (solid line) and phase contours (dashed line) every 20° of the K_1 constituent for E1 (left) and E2 (right) experiments

Table 5: Observed Amplitude (A_{ob}) and Phase (P_{ob}) and modeled Amplitude (A_{Ei}) and Phase (P_{Ei}) for K_1 elevation at 14 coastal locations

Stations	A_{ob}	A_{E1}	A_{E2}	P_{ob}	P_{E1}	P_{E2}
La goulette	3.0	3.8	3.7	195.7	215.0	210.8
Sfax	1.8	2.5	1.9	4.5	56.2	23.5
Gabes	2.5	2.6	2.2	349.3	316.9	356.3
SG	0.5	0.2	0.4	78.0	83.2	59.8
Palermo	2.9	3.8	4.1	199.2	185.6	184.5
Mazzara	3.5	3.2	4.2	85.5	118.5	114.9
Po. Emp	1.5	1.0	1.8	88.7	85.8	83.4
Valetta	1.1	1.1	1.4	28.5	14.5	9.7
C. passero	1.9	1.3	1.8	52.2	18.2	31.2
Lampedusa	0.6	0.9	0.9	346.6	309.8	359.1
Catania	1.6	1.3	1.8	42.1	27.8	37.6
Tropea	4.1	4.0	4.3	203.1	186.7	190.8
Milazzo	3.3	4.0	4.3	200.0	186.7	189.7
Lipari	3.1	4.0	4.3	199.0	187.0	189.6

characteristics of tides in the domain, researchers show in Table 2-5, the values of the observed and model amplitudes and phases as estimated by E1 and E2 experiments for M_2, S_2, N_2 and K_1 constituents for the tidal stations whose distribution is shown on Fig. 2. The O_1 amplitude seems to be close to the background noise level and because the errors in the observed tides used in this study were not estimated, we believe that the validation of the modelled O_1 harmonic constants against the observed ones must be taken with caution. The amplitude and phase of different tidal components are reasonably represented in E2 experiment and are far from data for E1 experiment showing the positive impact of the potential forcing and the load tide in improving the quality of model simulations.

In Fig. 7a, b, researcher plot the amplitude and phase predicted by these two experiments versus observed ones at tide-gauge stations for M_2 and K_1 constituents. The amplitudes and phases predicted by E2 experiments are in general much closer to data than those of E1 experiment. Since, the results provided by E2 experiment are better than those of E1, particularly in the amplification zone (Gulf of Gabes), researchers concentrate the model validation on the comparison of elevation as simulated by E2 versus observation. To this end and to provide a quantitative assessment of the elevation field, the root mean square (rms) amplitude and phase differences as well as the Root Mean Square Norm (RMSN) were computed for M_2, S_2, N_2 and K_1. The RMSN is given by:

$$RMSN=\sqrt{\frac{1}{2n}\sum_{i=1}^{n}(a_{mi}^2+a_{oi}^2-2a_{oi}a_{mi}\cos(p_{mi}-p_{oi}))}$$

Where:

n = Number of tide-gauge stations
a_{oi} and a_{mi} = The observed and modelled amplitudes
p_{oi} and p_{mi} = The observed and modelled phases

Table 6 shows the root-mean-square (rms) amplitude and phase differences between the modelled and observed amplitude and phase for each tidal component as well as the RMSN. The results compare favourably to data, since both amplitude and phase were given with reasonable accuracy and this could be a sufficient check of accuracy. Indeed, the agreement is quite good for the amplitudes with rms error of 1.7 cm (3% of the maximum

Table 6: Root mean square (rms) amplitude and phase differences between the modelled and observed amplitude and phase for each tidal component as well as the Root Mean Square Norm (RMSN)

Amplitude	M_2	S_2	N_2	K_1
rms (cm)	1.7	0.8	0.9	0.6
rms (°)	14.3	17.6	16.7	15.5
RMSN (cm)	1.6	1.1	0.5	0.5

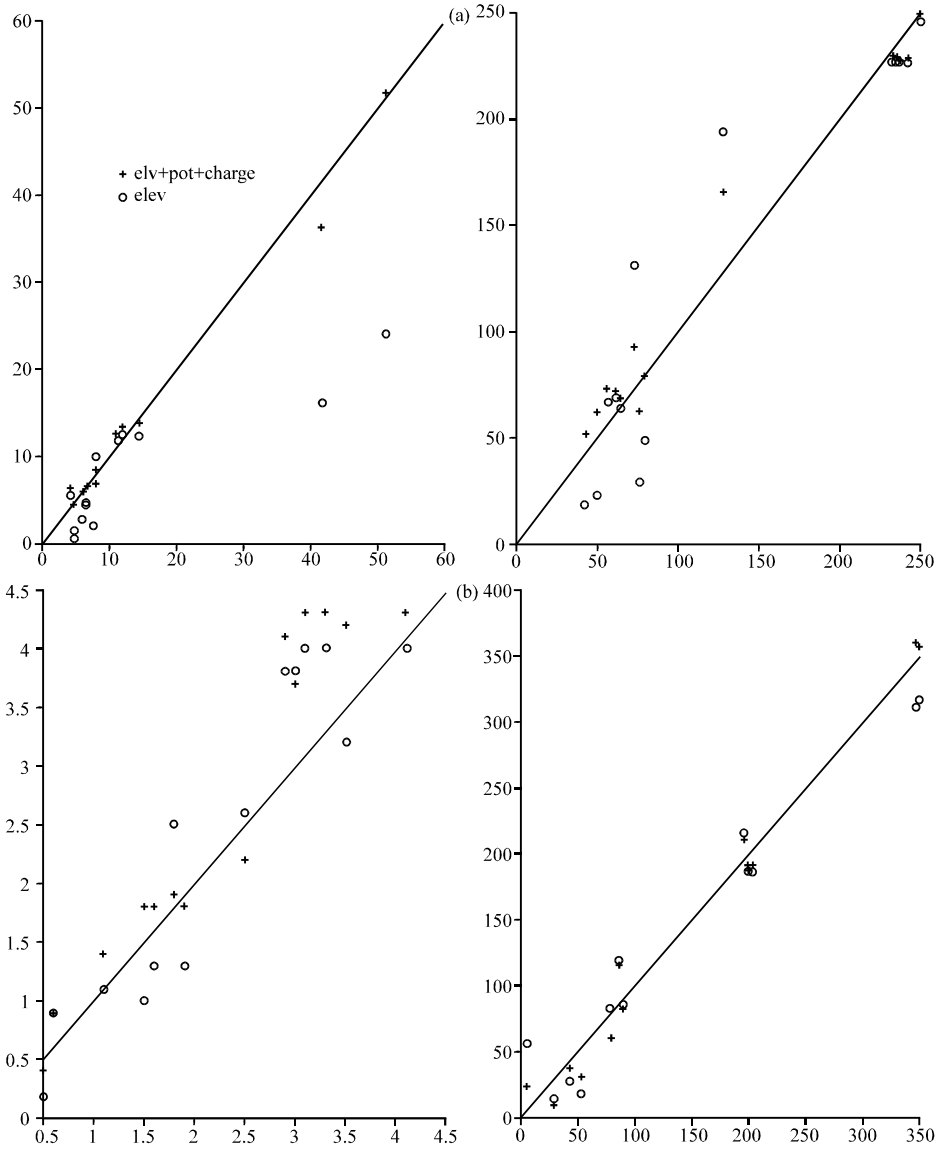

Fig. 7: a) Modelled amplitude (left) and phase (right) versus observed ones for M_2 constituent; b) for K_1 constituent. Line indicates tide gauge data, circles indicate results of E1 experiment and stars indicate results of E2 experiment

observed amplitude) for M_2, <1 cm for both S_2 and N_2 components and 0.6 cm for K_1 component. The modelled phases compare also reasonably to the observed ones. Indeed, the rms error shown in Table 6 is <18° for all modelled components. The presence of the amphidromic point near the SG station may explain the phase discrepancy for K_1 component. It is important to note that the rms error between observations and Mog2d model (used to force the model) was about 39° for K_1, an error much larger than that estimated from the simulations. According to the RMSN values, it appears that the local solution is very close to tide-gauge data which underlines the impact of the potential forcing particularly in the resonance region.

Researchers attribute the few cm error in amplitude particularly to the error in open boundaries forcing and to bathymetry uncertainties. Indeed, we conducted some simulations in which the open boundary forcing was adjusted (by increasing slightly the amplitude of elevation since, it is underestimated by Mog2d) in order to obtain a good agreement between the model solution and the tide gauge data. We found that computed elevation

amplitudes in the interior of the basin were increased even with small changes in the open boundaries forcing. This sensitivity study confirmed the importance of an accurate specification of tide along the open boundary. Nevertheless, it must be noted that all the results discussed here are obtained without any tuning of the harmonic constituents deduced from Mog2d.

CONCLUSION

Researchers have investigated the spatial distribution of M_2, N_2, S_2, K_1 and O_1 tidal constituents which are the most important in the Mediterranean sea (Purga *et al*., 1979). To this end, we used a high-resolution barotropic tidal model to predict tidal elevations and currents. Model performance was evaluated with respect to tide gauge measurements. In order to investigate the impact of the potential forcing on the local solution, we have conducted two numerical experiments. In the first one, the model is only forced by elevation at the open boundaries and in the second one we added the potential forcing. For both experiments, the model reproduces qualitatively well the spatial distribution of the modelled tidal components. On the hand, the modelled amplitude of elevation is underestimated in the resonance region when we consider only the forcing at the open boundaries. The addition of the potential forcing enhances the quality of the simulations, since the model fields faithfully reproduced the major features of the barotropic tide and had a reasonable agreement with the existing amplitude and phase observations. Indeed, the rms error does not exceed 1.7 cm for M_2 component and it is about 0.6 cm for K_1. Moreover, the maximum modelled amplitude (51.7 cm) is very close to the observed one (51.1 cm) in the resonance area. Nevertheless, the comparison between model and data amplitude and phase in different stations of measurements shows that there is no clear modification of the tidal characteristics outside the resonance region. Moreover, it seems that the impact of the potential forcing is particularly important within the semidiurnal frequency which is the resonance frequency in the Gulf of Gabes. The results suggest that the introduction of the generative potential could be important for improving a local solution especially in the case of a phenomenon of resonance. The various semidiurnal constituents which are the most important in the domain have nearly the same behaviour as each other. Each one has one amphidromic point and strong amplification on the Tunisian shelf with the maximum amplitude in the Gulf of Gabes. The diurnal constituents dominated by K_1 are generally weak but with high amplitude in the NW and SE of Sicily and with phase propagating from SE to NW.

The results for semidiurnal tides are more accurate than those for the diurnal ones. This is foreseeable since the tuning of the model was realised for M_2 which is the dominant tidal constituent in the basin. Moreover at the diurnal period, other local forcings such as wind and atmospheric pressure are possible and they can corrupt the observations, therefore contaminate K_1.

The uncertainties in boundary conditions and bathymetry are main sources of error for the model. We believe that more realistic tidal forcing and bathymetry enhance the results reliability. The results suggest that the potential forcing should be introduced even in the local solution, particularly in the resonance area. Finally, we believe that even though the barotropic simulations are subject to some errors, they would be very helpful to tune larger tidal models of the Mediterranean sea.

ACKNOWLEDGEMENTS

The researchers are supported by Ministere de l'Enseignement Superieur et de la Recherche Scientifique through l'Unite de Recherche 01UR1304.

REFERENCES

Abdennadher, J. and M. Boukthir, 2006. Numerical simulation of the barotropic tides in the tunisian shelf and the strait of sicily. J. Marine Syst., 63: 162-182.

Astraldi, M., C. Galli, G.P. Gasparini, E. Lazzoni and G.M.R. Manzella, 1987. The Janus experiment. Internal Report, TR 140, CNR/CREA, La Spezia, Pages: 38.

Candela, J., C. Winant and A. Ruiz, 1995. Tides in the Strait of Gibraltar. J. Geophys. Res., 95: 7313-7335.

Defant, A., 1961. Physical Oceanography. Pergamon Press, Oxford, England, Pages: 598.

Gallagher, B.S. and W.H. Munk, 1971. Tides in shallow water: Spectroscopy. Tellus, 23: 346-363.

Le Provost, C., M.L. Genco, F. Lyard, P. Vincent and P. Canceil, 1994. Spectroscopy of the world ocean tides from a finite element hydrodynamic model. J. Geophys. Res., 99: 24777-24798.

Lozano, C.J. and J. Candela, 1995. The M2 tide in the Mediterranean Sea: Dynamic analysis and data assimilation. Oceanol. Acta., 18: 419-441.

Molines, J.M., 1991. Modeling the barotropic tides in the strait of Sicily and Tunisian coasts. Oceanol. Acta., 14: 241-251.

Mosetti, R., F. Mosetti and N. Purga, 1983. On some short period tides in the seas around Italy. Boll. Oceanol. Teor. Appl., 1: 49-66.

Munk, W.H. and C. Wunsch, 1998. Abyssal recipes II: Energetics of tidal and wind mixing. Deep Sea Res., 45: 1977-2010.

Parker, B.B., 1991. Tidal Hydrodynamics. John Wiley and Sons, New York, Pages: 883.

Purga, N., F. Mosetti and E. Accerboni, 1979. Tidal harmonic constants for some Mediterranean harbours. Boll. Geofis. Teor. Appl., 21: 72-81.

Sanchez, B.V., R.D. Ray and D.E. Cartwright, 1992. A Proudman-function expansion of the M2 tide in the Mediterranean Sea from satellite altimetry and coastal gauges. Oceanol. Acta., 15: 325-337.

Shchepetkin, A.F. and J.C. McWilliams, 2003. A method for computing horizontal pressure-gradient force in an ocean model with a non-aligned vertical coordinate. J. Geophys. Res., 108: 3501-3534.

Smith, W.H.F. and D.T. Sandwell, 1997. Global sea floor topography from satellite altimetry and ship depth soundings. Science, 227: 1956-1962.

Tsimplis, M.N., 1994. Tidal oscillations in the Aegean and Ionian Seas. Estuarine Coastal Shelf Sci., 39: 201-208.

Tsimplis, M.N., R. Proctor and R.A. Flather, 1995. A two-dimensional tidal model for the Mediterranean Sea. J. Geophys. Res., 100: 16223-16239.